IRANIAN JOURNAL OF CATALYSIS

The formate and redox mechanisms of water-gas shift reaction on the surface of Ag: A nanocluster model based on DFT study

Darioush Sharafie, Ali Arab*, Mostafa Fazli

Department of Chemistry, Semnan University, Semnan, Iran.

ABSTRACT

Two different possible mechanisms of water gas shift reaction including formate and redox mechanisms on the Ag_5 cluster were investigated using DFT computations. All the elementary steps involved in both mechanisms were considered. It was observed that dissociation of H_2O_{ads} and OH_{ads}, as well as formation of $CO_{2(ads)}$, required activation energy. For these steps, transition state structures were determined and their corresponding activation energies were calculated. For both mechanisms, the highest activation energy (402.34 kJ mol^{-1}) was related to the dissociation of OH_{ads} as the rate limiting step. The calculated activation energy of $CO_{2(ads)}$ formation according to the redox mechanism ($CO_{ads} + O_{ads} \rightarrow CO_{2(ads)}$) was 9.32 kJ mol^{-1} indicating that this step was relatively fast on the surface of Ag_5 cluster. It was observed that, $CO_{2(ads)}$ formation according to the formate mechanism occurred through three consecutive steps where the dissociation of formate ($HCOO_{(ads)} \rightarrow CO_{2(ads)} + H_{ads}$) had the highest activation energy, 171.53 kJ mol^{-1}.

Keywords: Density functional calculations, Kinetics, Reaction mechanisms, Silver cluster.
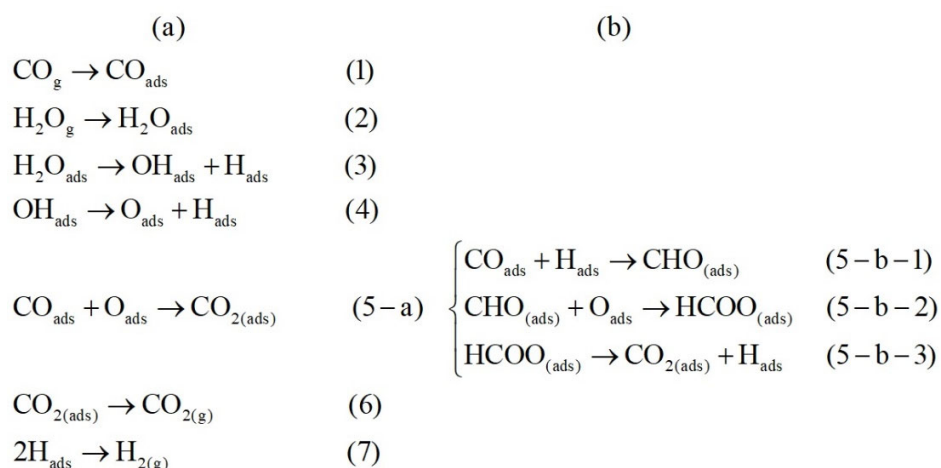
1. Introduction

The water gas shift reaction (WGSR), $CO + H_2O \rightarrow CO_2 + H_2$, is one of the most important reactions in the industry for hydrogen generation and CO removal. The production of hydrogen from various sources will lead to the development of the world through the hydrogen economy. In fact, WGSR is an intermediate reaction for the production of carbon-based hydrogen [1-7]. It is believed that WGSR begins with the dissociation of water [8-10] and then proceeds in different paths depending on the reaction of CO with different generated species [11]. Due to the specific importance of WGSR, abundant experimental and computational studies have been devoted to find its mechanism and better catalysts. These studies have shown that the WGSR mainly proceeds via three mechanisms including carboxyl, redox and formate pathways depending on the employed catalysts [12-14]. In the theoretical study of WGSR, nanoclusters have attracted considerable attention [15-18]. The catalytic performance of nanoparticles and real catalysts can be estimated by studying the interaction between nanoclusters and reactant species [18-21]. Ag nanoclusters with interesting physical and chemical properties are applicable for different catalytic reactions [22-24]. For example, TiO_2 surfaces incorporated with Ag clusters have good catalytic activity for N_2O dissociation [23] and p-nitrophenol reduction [24].

The carboxyl mechanism of WGSR on the surface of Ag nanocluster was analyzed in our previous study and results revealed that dissociation of H_2O was the rate limiting step [15]. In addition, according to our results, Ag cluster showed good catalytic activity for H_2O dissociation compared to the Ni, Cu, and Au clusters. In the present paper, the other mechanisms of WGSR including redox [25] and formate [7] as presented in scheme 1 were investigated on the silver nanocluster using DFT calculations. The transition states, energy profiles, and kinetics of each step were completely determined and discussed. The aim of this study is to promote future researches relating to WGSR catalysts. In addition, the NBO results and Wiberg bond indexes were analyzed in order to better investigate the nature of the interaction between reactants, products, and transition states with the silver cluster.

---

*Corresponding author.
E-mail address: a.arab@semnan.ac.ir (A. Arab)

(a)   (b)

$$CO_g \rightarrow CO_{ads} \quad\quad (1)$$

$$H_2O_g \rightarrow H_2O_{ads} \quad\quad (2)$$

$$H_2O_{ads} \rightarrow OH_{ads} + H_{ads} \quad\quad (3)$$

$$OH_{ads} \rightarrow O_{ads} + H_{ads} \quad\quad (4)$$

$$CO_{ads} + O_{ads} \rightarrow CO_{2(ads)} \quad\quad (5-a)$$

$$\begin{cases} CO_{ads} + H_{ads} \rightarrow CHO_{(ads)} & (5-b-1) \\ CHO_{(ads)} + O_{ads} \rightarrow HCOO_{(ads)} & (5-b-2) \\ HCOO_{(ads)} \rightarrow CO_{2(ads)} + H_{ads} & (5-b-3) \end{cases}$$

$$CO_{2(ads)} \rightarrow CO_{2(g)} \quad\quad (6)$$

$$2H_{ads} \rightarrow H_{2(g)} \quad\quad (7)$$

Scheme 1. The proposed redox [25] (a) and formate [7] (b) mechanisms of water gas shift reaction.

2. Computational details

Density functional theory (DFT) computations at the hybrid B3PW91 functional [26, 27] were employed for all of the analyses. The B3PW91 functional is reported as an acceptable functional for investigation of small clusters [28-32]. For example, the results obtained using B3PW91 functional for silver small clusters are in good accordance with the results obtained using more accurate coupled-cluster (CCSD) methods [28-30]. For O, C, and H atoms, the 6-31+G* and for Ag atom, the LANL2DZ (with effective core potential) basis sets were used. Geometry optimization was followed by the frequency analysis in order to evaluate the nature of optimized structures. The intrinsic reaction coordinate (IRC) analysis was employed to corroborate that an obtained saddle point connects two considered minima. For the calculation of thermodynamic quantities, all of the energies were corrected by considering the zero-point energy contribution. The natural bond orbital (NBO) analysis was also applied to the optimized structures. All of the computations were carried out using the Gaussian 03 program [33].

3. Results and Discussion

Different geometries for Ag_5 cluster were optimized and the most stable geometry was a quasi-planer geometry with the spin multiplicity of 2 [15]. This geometry was considered here for the investigation of all steps included in the redox and formate mechanisms (see scheme 1) as follows:

3.1. Adsorption of H_2O and CO

Adsorption of CO from carbon and oxygen ends on different sites of Ag_5 cluster was investigated. The most stable geometry as presented in Fig. 1 (a) is adsorption from the carbon atom on the top site of Ag_5 cluster. In this geometry, the obtained values of adsorption energy and the nearest distance between carbon and silver atom of the cluster are -12.53 kJ mol^{-1} and 2.236 Å, respectively.

The values of adsorption energies were evaluated using Eq. 1

$$E_{ads} = E_{cluster-adsorbed} - E_{cluster} - E_{adsorbed} \quad (1)$$

Where $E_{adsorbed}$, $E_{cluster}$, and $E_{cluster-adsorbed}$ denote energy of the adsorbed entity, cluster and cluster-adsorbed complexes, respectively.

The covalent character of a bond can be explained using the Wiberg bond index (WBI). The larger values of WBI show the stronger covalent character. The WBI values were obtained from the NBO calculations.

The NBO charges on Ag_3 atom before and after CO adsorption are 0.04 and -0.10, respectively. The NBO charges of C and O atoms before adsorption are 0.51 and -0.51 and after adsorption are 0.48 and -0.44, respectively. In addition, the WBI of CO after adsorption has been reduced from 2.25 to 2.22. These results indicate that charge transfer has occurred from the bonding orbitals of CO to the Ag_5 cluster.

According to the NBO results, no natural bond orbital (BD) was observed between the carbon atom of CO and the silver atom(s) of the cluster indicating no typical covalent C-Ag bond [34]. For C-Ag and Ag-Ag bonds, the obtained WBIs are smaller than 1 indicating that the interactions involved in the C-Ag and Ag-Ag bonds are weak compared to a covalent single bond. In other words, electrostatic interactions have more contribution to the C-Ag and Ag-Ag bonds [35, 36].

Fig. 1 (b) exhibits the most stable state of adsorbed H_2O on the Ag_5 cluster. In this structure, H_2O prefers to adsorb from the oxygen end on the top site of Ag_5 cluster and its adsorption energy is -13.5 kJ mol^{-1}.
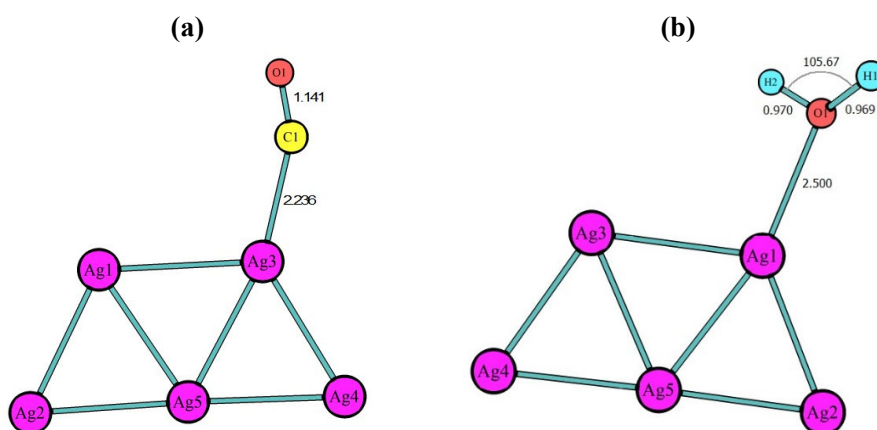
(a)   **(b)**

Fig. 1. The most stable adsorption modes of CO (a) and H_2O (b) on Ag_5 cluster.

This optimized geometry is the reactant of $H_2O_{ads} \rightarrow H_{ads} + OH_{ads}$ step in order to find the transition state structure. The NBO atomic charges of H atoms are obtained 0.49 and 0.51 before and after adsorption, respectively. For O atom, no variation in NBO charge (-0.98) is observed after adsorption. The WBI of O-H bonds has been reduced from 0.76 to 0.73 after adsorption. Therefore, the charge transfer has occurred form the bonding orbitals of OH to the Ag_5 cluster. The obtained value of WBI for the O-Ag_1 bond is 0.10 confirming there is no typical covalent bond between cluster and H_2O.

The above results reveal that H_2O and CO entities were adsorb physically on the Ag_5 cluster so that the initial steps of redox and formate mechanisms are spontaneous.

3.2. Dissociation of H_2O

OH and H co-adsorption on the Ag_5 cluster is studied to provide kinetic information for $H_2O_{ads} \rightarrow H_{ads} + OH_{ads}$ step. The most stable configuration of OH & H co-adsorbed (E_{ads}=-445.37 kJ mol^{-1}) on the Ag_5 cluster as the product of the step is displayed in Fig. 2. The geometry of transition state and energy barrier of this step are determined and results are presented in Fig. 2. The WBI of O1-H2 bond has been reduced from 0.73 in the reactant to 0.15 in the geometry of transition state. In addition, in the geometry of transition state, a new bond with WBI of 0.35 has been formed between Ag3 and H2 atoms. In the product, the WBIs of O1-Ag1, O1-Ag3, H2-Ag3, and H2-Ag4 bonds are 0.20, 0.24, 0.46, and 0.30, respectively.
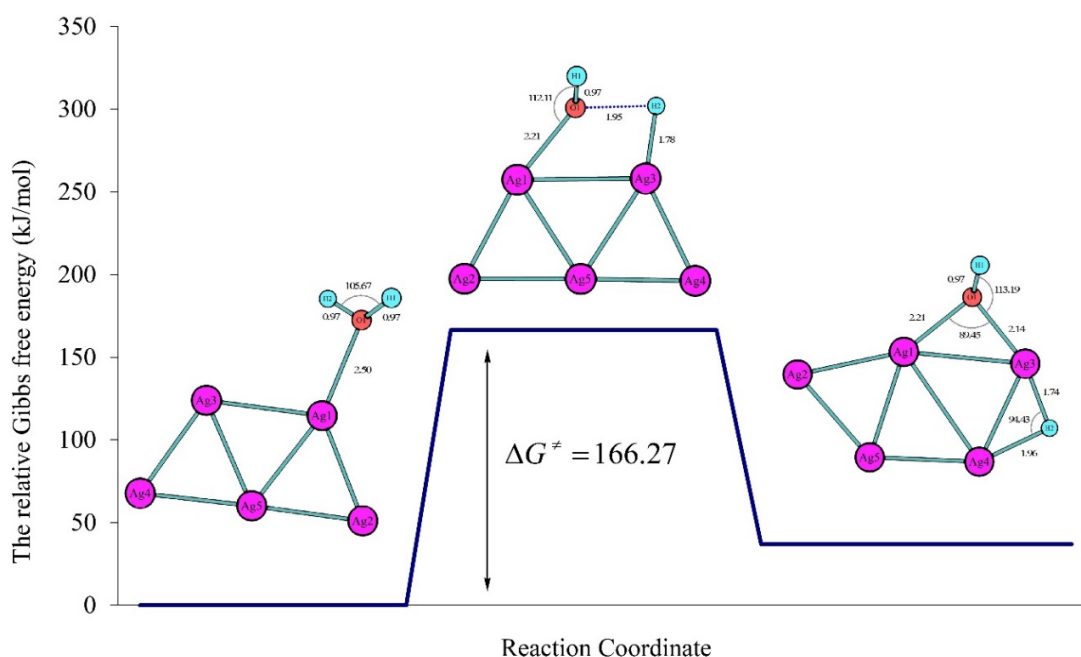

Fig. 2. The energy barrier of H_2O_{ads} dissociation on the Ag_5 cluster according to the $H_2O_{ads} \rightarrow H_{ads} + OH_{ads}$ reaction.

The free energy of activation ($\Delta G^{\neq}$) for H_2O_{ads} dissociation on the Ag_5 cluster is obtained to be 166.27 kJ mol^{-1}. The comparable results have also been reported for the activation energy of H_2O_{ads} dissociation on different catalysts [18, 37, 38]. For example, the values of 87.90 kJ mol^{-1} and 137 kJ mol^{-1} have been obtained for the activation energy of H_2O dissociation on the Pt_4 cluster [18] and on the surface of ZnO supported by 2Cu atoms [37], respectively. For bimetallic clusters of copper (Cu_{12}-M, M= Au, Ag, Ni, and Cu) the values of 123.39 kJ mol^{-1}, 110.85 kJ mol^{-1}, 108.93 kJ mol^{-1}, and 109.89 kJ mol^{-1} have been obtained for M= Au, Ag, Ni, and Cu, respectively as the activation energy of H_2O dissociation [38]. On the Au_{10}, Au_{13}, and Au_{20} clusters, the values of 276.00 kJ mol^{-1}, 169.84 kJ mol^{-1}, and 204.85 kJ mol^{-1} have been reported as the activation energy for H_2O dissociation [39].

The rate constant of this step ($k = 4.60 \times 10^{-17} S^{-1}$) was calculated according to the Eq. 2.

$$k = \frac{K_B T}{h} exp\left(-\frac{\Delta G^{\neq}}{RT}\right) \qquad (2)$$

Where K_B, T, h, and R are the Boltzmann constant, temperature (298 K), the Planck constant, and gas constant, respectively.

3.3. Dissociation of OH

OH_{ads} intermediate dissociates to the O_{ads} and H_{ads} entities by the $OH_{ads} \rightarrow O_{ads} + H_{ads}$ reaction. Adsorption of OH as the reactant and also O&H co-adsorption as the product of this step are investigated on the Ag_5 cluster. Fig. 3 presents the structures with the lowest energy for the reactant, product and transition state along with the corresponding energy barrier of this step. For the adsorption of OH and co-adsorption of H&O species on the Ag_5 cluster, the values of adsorption energies are obtained -287.27 kJ mol^{-1} and -660.34 kJ mol^{-1}, respectively. The WBIs of O1-Ag1, O1-Ag3, and O1-H1 bonds are 0.20, 0.20, and 0.76 in the reactant and 0.62, 0.24, and 0.33 in the transition state, respectively. A new bond between the Ag1 and H1 atoms of the transition state has also been formed with the WBI of 0.56. Furthermore, in the product, the calculated WBIs of O1-Ag1, O1-Ag3, Ag2-H1, and Ag1-H1 bonds are 0.55, 0.33, 0.38, and 0.39, respectively. For this step, the highest value (402.34 kJ mol^{-1}) for activation energy ($\Delta G^{\neq}$) is obtained. In addition, the calculated value of rate constant (k) for this step is $2.01 \times 10^{-58} S^{-1}$. Therefore, dissociation of OH_{ads} intermediate is the rate determining step of redox and formate mechanisms and O_{ads} and H_{ads} species are slowly formed on the Ag_5 cluster. The values of 480.57 kJ mol^{-1}, 234.50 kJ mol^{-1}, and 482.50 kJ mol^{-1} have been reported for the activation energy of OH_{ads} dissociation on Au_{10}, Au_{13}, and Au_{20} clusters, respectively [39].

3.4. $CO_{2(ads)}$ formation from redox mechanism

In the redox mechanism, the oxidation of CO is done by atomic O obtained from dissociation of OH (step 4 of scheme 1), to form CO_2 according to the step (5-a) presented in scheme 1. The most stable geometries of O&CO species co-adsorbed (E_{ads}= -545.62 kJ mol^{-1}) and CO_2 adsorbed (E_{ads}= 45.31 kJ mol^{-1}) on the cluster have been shown in Fig. 4 as the reactant and product, respectively.

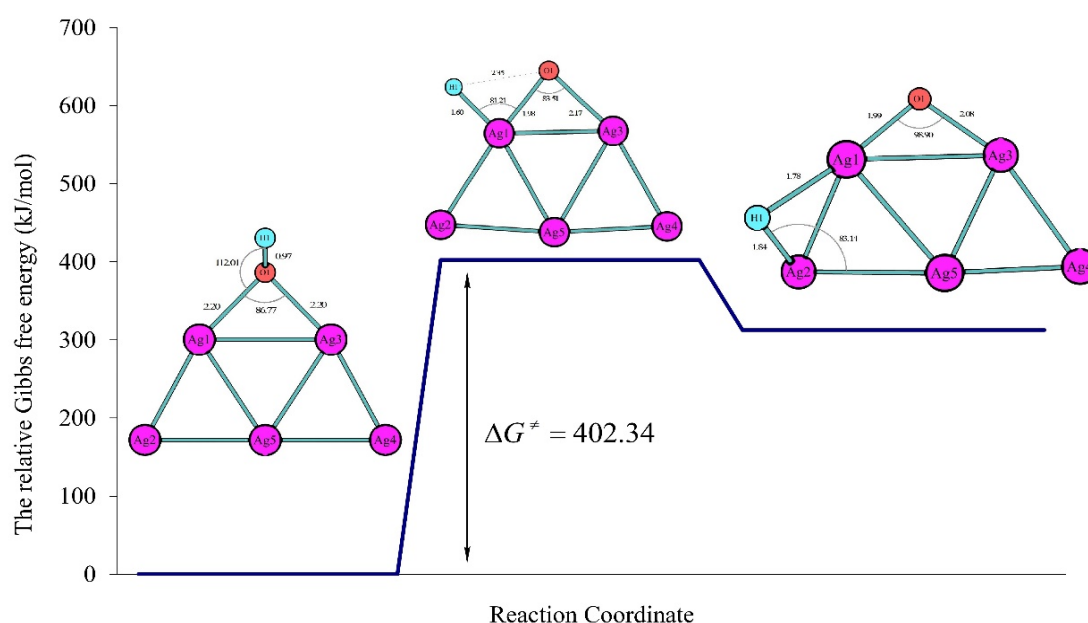**Fig. 3.** The energy barrier of OH_{ads} dissociation on the Ag_5 cluster according to the $OH_{ads} \rightarrow O_{ads} + H_{ads}$ reaction.
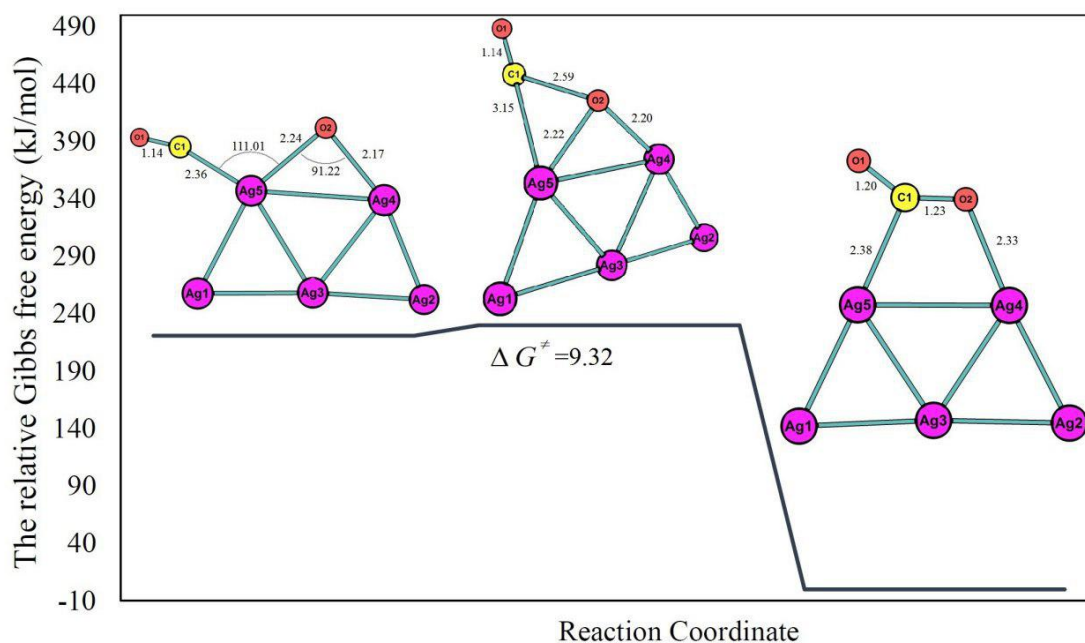
Fig. 4. The energy barrier of $CO_{ads} + O_{ads} \rightarrow CO_{2(ads)}$ step on the Ag₅ cluster according to the redox mechanism.

The optimized geometry of the transition state along with the corresponding energy barrier is also presented in Fig. 4. In the reactant, the WBIs of C1-O1, C1-O2, C1-Ag5, O2-Ag4, O2-Ag5, Ag4-Ag5 bonds are 2.26, 0.01, 0.38, 0.24, 0.25, and 0.06, respectively. In the transition state, the WBIs of O2-Ag4, O2-Ag5, C1-Ag5, and C1-O1 bonds have been reduced to 0.21, 0.21, 0.10, and 2.24, respectively while the WBIs of C1-O2 and Ag5-Ag4 bonds have been increased to 0.06 and 0.08 respectively compared to the reactant. In the product, the WBIs of C1-O1, C1-O2, C1-Ag5, O2-Ag4, O2-Ag5, Ag4-Ag5 bonds are 1.73, 1.52, 0.25, 0.11, 0.04, and 0.11, respectively. For this step, the calculated values of $\Delta G^{\neq}$ and rate constant (k) are 9.32 kJ mol⁻¹ and $1.45 \times 10^{11}\ S^{-1}$, respectively. It indicates that CO₂(ads) formation according to the redox mechanism is a fast reaction on the silver cluster. A similar result has also been reported for the formation of CO₂(ads) on copper [25]. On the Pt₄ cluster, on the other hand, a high activation energy (114.20 kJ mol⁻¹) has been obtained for the formation of CO₂(ads) [18]. On the Au₁₀, Au₁₃, and Au₂₀ clusters, the values of 331.00 kJ mol⁻¹, 117.73 kJ mol⁻¹, and 30.88 kJ mol⁻¹ have been obtained for the activation energy of OH(ads) dissociation [39].

3.5. CO₂(ads) formation from formate mechanism

For the formation of CO₂(ads) according to the formate mechanism, three consecutive steps (5-b-1), (5-b-2), and (5-b-3) of scheme 1 occur. In (5-b-1) step, CO(ads) reacts with the H(ads) obtained from dissociation of OH (step 4 of scheme 1) to form CHO(ads),

$CO_{ads} + H_{ads} \rightarrow CHO_{(ads)}$. Co-adsorption of CO and H species and the adsorption of CHO have been investigated on the Ag₅ cluster as the reactant and product, respectively. The adsorption energies for co-adsorbed H&CO and adsorbed CHO on the Ag₅ cluster are obtained -253.53 kJ mol⁻¹ and -102.18 kJ mol⁻¹, respectively. The most stable structures of reactant, transition state, and product of this step have been presented in Fig. 5. The WBI values of C1-H1 bond in the reactant, transition state, and product are 0.03, 0.45, and 0.68, respectively. For, H1-Ag3 bond, the obtained values of WBI are 0.36, 0.02, and 0.24 for the reactant, product, and transition state, respectively. For this step, the calculated values of $\Delta G^{\neq}$ and rate constant (k) are 73.81 *kJ mol⁻¹* and $7.27 \times 10^{-1} S^{-1}$, respectively.

In (5-b-2) step, the formate specie (HCOO) has been formed according to the $CHO_{(ads)} + O_{ads} \rightarrow HCOO_{(ads)}$ elementary reaction. Co-adsorption of CHO&O species as the reactant is investigated on the Ag₅ cluster and two different structures (R1, R2 of Fig. 6) are optimized. In this figure, the values of the relative (E_r) and adsorption (E_{ads}) energies are also presented. The transition states of this step are determined considering both R1 and R2 structures as the reactant. The relative energies show that the R2 structure is 24.10 kJ mol⁻¹ less stable than R1 structure. For the adsorption of HCOO entity on the cluster, three different structures as the products are optimized (P1, P2, and P3 of Fig. 6). The P1 structure is 10.60 kJ mol⁻¹ and 32.78 kJ mol⁻¹ more stable than P2 and P3 structures, respectively.
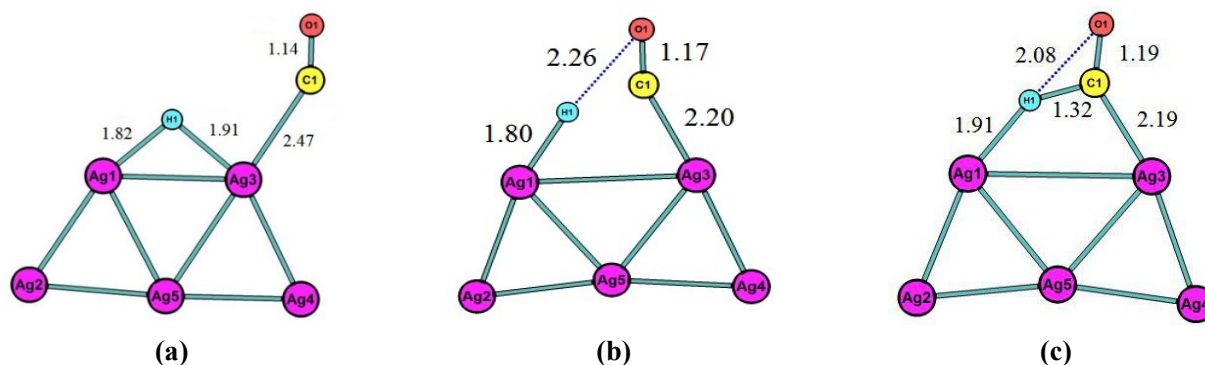
Fig. 5. The most stable structures of reactant (a), transition state (b), and product (c) of $CO_{ads} + H_{ads} \rightarrow CHO_{(ads)}$ reaction on the Ag_5 cluster.

For the conversion of R1 and R2 structures to the P1, P2 and P3 structures three different transition states (ts1, ts2, and ts3 of Fig.6) and four different paths (Fig. 7) are obtained. The ts1 structure is 38.56 kJ mol^{-1} and 52.06 kJ mol^{-1} more stable than ts2 and ts3 structures, respectively. The caclculated values of free energies of activation ($\Delta G^{\neq}$) and rate constants (k) for the four paths presented in Fig. 7 have been collected in Table 1. The smallest value of activation energy is related to the R1-P1 and R1-P2 paths, 7.78 kJ mol^{-1}. For R1-P1 and R1-P2 paths, similar transition state is obtained (ts1 of Fig. 6) but the P1 product is 10.60 kJ mol^{-1} more stable than the P2 product.

In the formate mechanism, the $CO_{2(ads)}$ is formed from the dissociation of formate species according to the (5-b-3) step, $HCOO_{(ads)} \rightarrow CO_{2\,(ads)} + H_{ads}$. The considered reactants for this step are the products of the previous step (P1 and P3 of Fig. 6). For the product of this step, Co-adsorption of H&CO$_2$ species is investigated on Ag$_5$ cluster and the optimized structure (P) is presented in Fig. 8. Two optimized geometries of transition states (ts1 and ts2) of this step are also shown in Fig. 8. The ts1 structure is 28.92 kJ mol^{-1} more stable than ts2 structure. For this step, two energy barriers have also been obtained for the conversion of reactants (P1 or P3) to the product (P) as presented in Fig. 9. The calculated values of free energies of activation ($\Delta G^{\neq}$) for P3-P and P1-P paths are 167.55 kJ mol^{-1} and 171.53 kJ mol^{-1}, respectively. The corresponding values of rate constants are obtained $2.74 \times 10^{-17} S^{-1}$ and $5.51 \times 10^{-18} S^{-1}$ for P3-P and P1-P paths, respectively. Therefore, dissociation of formate has a higher activation barrier compared to its formation (167.55 kJ mol^{-1} versus 7.78 kJ mol^{-1}). This confirms that formate entity is a stable and observable intermediate in the WGSR in accordance with the experimental observations [14].

As can be seen in scheme 1, the evolution of carbon dioxide and hydrogen are the termination steps of both redox and formate mechanisms. The values of ΔG for these steps are obtained to be -17.72 kJ mol^{-1} and -41.52 kJ mol^{-1}, respectively. Therefore, it is clear that $CO_{2(ads)}$ and H_{ads} desorption are spontaneous processes on the Ag$_5$ cluster.

4. Conclusions

The redox and formate mechanisms of WGSR on the Ag$_5$ cluster were investigated by DFT calculations. All elementary reactions involved in both mechanisms were considered separately. The nature of the interaction between reactants, products, and transition states with the cluster was investigated using NBO analysis and calculation of Wiberg bond indexes. For both mechanisms, it is observed that some elementary reactions such as CO and H$_2$O adsorption and $CO_{2(ads)}$ and H$_{ads}$ desorption occurred spontaneously. For dissociation of H$_2$O$_{ads}$, dissociation of OH$_{ads}$, and formation of $CO_{2(ads)}$, the transition state geometries and energy barriers were determined. The free energy of activation ($\Delta G^{\neq}$) for H$_2$O$_{ads}$ and OH$_{ads}$ dissociation on the Ag$_5$ cluster was obtained to be 166.27 kJ mol^{-1} and 402.34 kJ mol^{-1}, respectively. Our kinetics results revealed that for both mechanisms dissociation of OH$_{ads}$ was the rate determining step. The formation of $CO_{2(ads)}$ which proceeds via different steps in the redox and formate mechanisms was also analyzed. According to the redox mechanism, $CO_{2(ads)}$ formation ($CO_{ads} + O_{ads} \rightarrow CO_{2\,(ads)}$) was a fast elementary step on the cluster with the activation energy of 9.32 kJ mol^{-1}. In the formate mechanism, $CO_{2(ads)}$ formation occurred through three steps containing formation and subsequent dissociation of formate intermediate ($HCOO_{(ads)}$). The formation of formate was a fast step (activation energy of 7.78 kJ mol^{-1}) compared to its dissociation (activation energy of 171.53 kJ mol^{-1}). This result confirmed that formate entity was an observable intermediate in accordance with the experimental observations.

R1
E_r= 0.00
E_{ads}= -916.76

R2
E_r= 24.10
E_{ads}= -892.66

ts1
E_r= 0.00

ts2
E_r= 38.56

ts3
E_r= 52.06

P1
E_r= 0.00
E_{ads}= -198.58

P2
E_r= 10.60
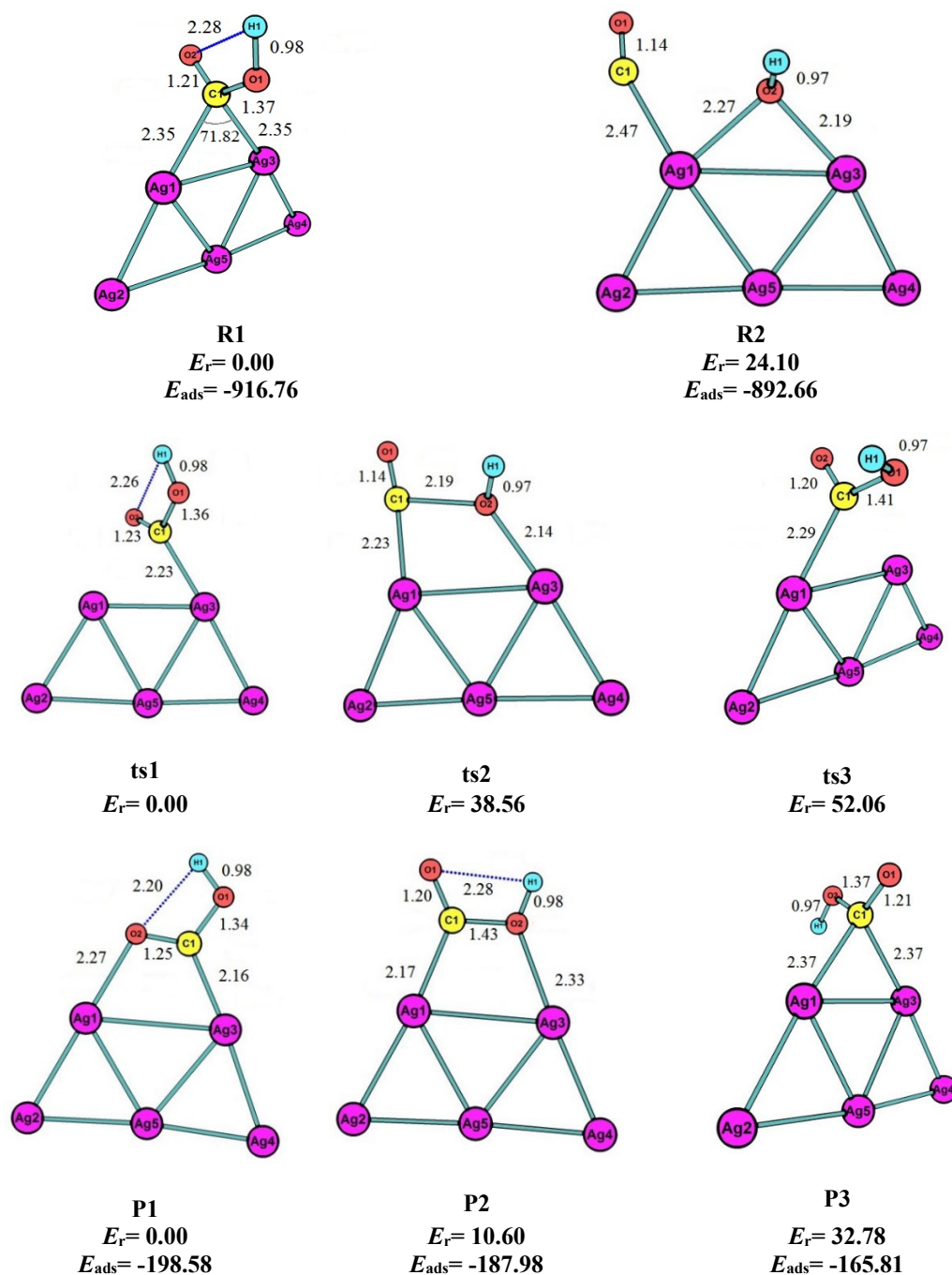E_{ads}= -187.98

P3
E_r= 32.78
E_{ads}= -165.81

Fig. 6. Different optimized structures, relative and adsorption energies of reactant (R1, R2), transition state (ts1, ts2), and product (P1-P3) of $CHO_{(ads)} + O_{ads} \rightarrow HCOO_{(ads)}$ step on the Ag$_5$ cluster. All energies are in kJ mol^{-1}.

Table 1. The calculated values of the free energies of activation ($\Delta G^{\neq}$) and rate constants (k) for different paths of $CHO_{(ads)} + O_{ads} \rightarrow HCOO_{(ads)}$ step presented in Fig. 7.

Path	$\Delta G^{\neq} (kJ/mol)$	$k\ (s^{-1})$
R1-P1	7.78	2.69×10^{11}
R1-P3	51.86	5.10×10^3
R1-P2	7.78	2.69×10^{11}
R2-P2	20.14	1.84×10^9
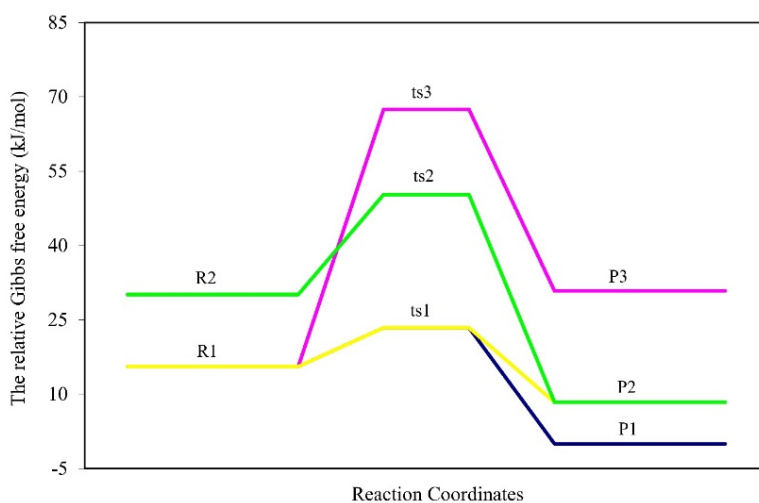
Fig. 7. Different energy barriers of $CHO_{(ads)} + O_{ads} \rightarrow HCOO_{(ads)}$ step on the Ag$_5$ cluster.

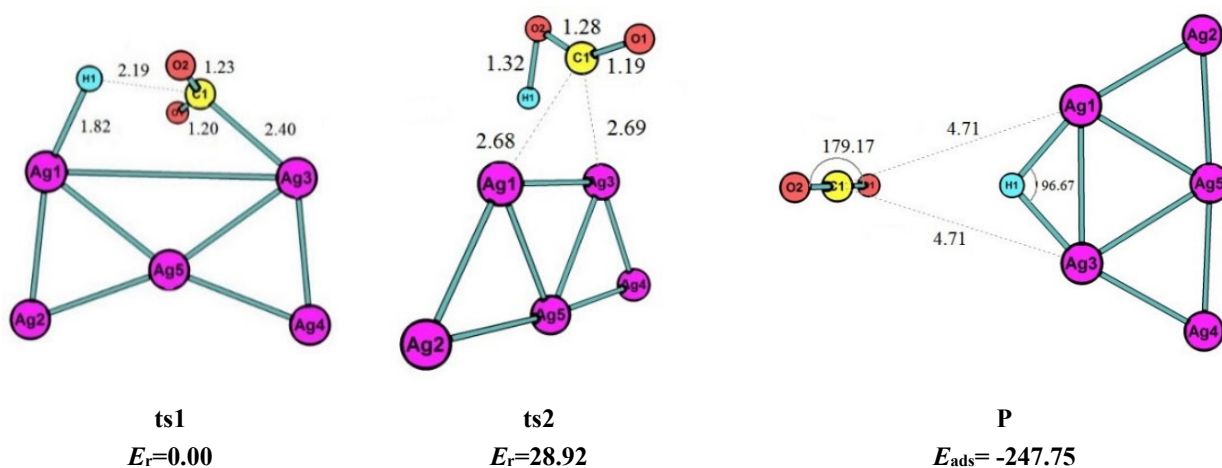|		
ts1	**ts2**	**P**
E_r=0.00	E_r=28.92	E_{ads}= -247.75

Fig. 8. Different optimized structures, relative and adsorption energies of the transition states (ts1, ts2) and product (P) of $HCOO_{(ads)} \rightarrow CO_{2(ads)} + H_{ads}$ step on the Ag$_5$ cluster. All energies are in kJ mol^{-1}.
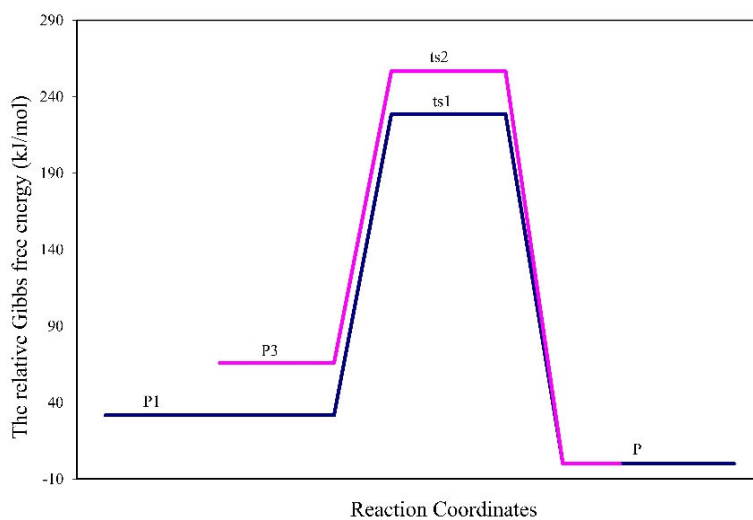

Fig. 9. Different energy barriers of $HCOO_{(ads)} \rightarrow CO_{2(ads)} + H_{ads}$ step on the Ag$_5$ cluster.

Acknowledgments

References

[1] J. Yu, F.J. Tian, M.C. Chow, L.J. McKenzie, C.Z. Li, Fuel. 85 (2006) 127-133.

[2] A.Y. Rozovskii, G.I. Lin, Top. Catal. 22 (2003) 137-150.

[3] S.H.D. Lee, D.V. Applegate, S. Ahmed, S.G. Calderone, T.L. Harvey, Int. J. Hydrogen Energ. 30 (2005) 829-842.

[4] D.S. Newsome, Catal. Rev. Sci. Eng. 21 (1980) 275-318.

[5] J. Sehested, Catal. Today 111 (2006) 103-110.

[6] D.W. Goodman, R.D. Kelley, T.E. Madey, J.T. Yates, J. Catal. 63 (1980) 226-234.

[7] J. Nakamura, J.M. Campbell, C.T. Campbell, J. Chem. Soc. Faraday Trans. 86 (1990) 2725-2734.

[8] C. Callaghan, I. Fishtik, R. Datta, M. Carpenter, M. Chmielewski, A. Lugo, Surf. Sci. 541 (2003) 21-30.

[9] I. Fishtik, R. Datta, Surf. Sci. 512 (2002) 229-254.

[10] G.C. Wang, L. Jiang, Z.S. Cai, Y.M. Pan, X.Z. Zhao, W. Huang, K.C. Xie, Y.W. Li, Y.H. Sun, B. Zhong, J. Phys. Chem. B 107 (2003) 557-562.

[11] Z.J. Zhao, Z. Li, Y. Cui, H. Zhu, W.F. Schneider, W.N. Delgass, F. Ribeiro, J. Greeley, J. Catal. 345 (2017) 157-169.

[12] R.C. Catapan, A.A. Oliveira, Y. Chen, D.G. Vlachos, J. Phys. Chem. C 116 (2012) 20281-20291.

[13] C. Ratnasamy, J.P. Wagner, Catal. Rev. 51 (2009) 325-440.

[14] C.H. Lin, C.L. Chen, J.H. Wang, J. Phys. Chem. C 115 (2011) 18582-18588.

[15] A. Arab, D. Sharafie, M. Fazli, J. Phys. Chem. Solids 109 (2017) 100-108.

[16] R.J. Lin, H.L. Chen, S.P. Ju, F.Y. Li, H.T. Chen, J. Phys. Chem. C 116 (2012) 336-342.

[17] S.K. Wu, R.J. Lin, S. Jang, H.L. Chen, S.M. Wang, F.Y. Li, J. Phys. Chem. C 118 (2014) 298-309.

[18] X. Lian, W. Guo, J. Shu, X. Zhang, Z. Liu, Y, Zhang, R. Liu, Theor. Chem. Acc. 134 (2015) 19.

[19] A. Arab, M. Habibzadeh, J. Nanostruct. Chem. 134 (2016) 111-119.

[20] A. Arab, M. Nahali, F. Gobal, J. Alloy Compd. 695 (2017) 1924-1929.

[21] A. Arab, M. Habibzadeh, Comput. Theor. Chem. 1068 (2015) 52-56.

[22] A.M. Shor, S.S. Laletina, E.A.I. Shor, V.A. Nasluzov, V.I. Bukhtiyarov, N. Rosch, Surf. Sci. 630 (2014) 265-272.

[23] M. Sowmiya, K. Senthilkumar, Appl. Surf. Sci. 389 (2016) 1220-1232.

[24] X. Wang, Z. Zhao, D. Ou, B. Tu, D. Cui, X. Wei, M. Cheng, Appl. Surf. Sci. 385 (2016) 445-452.

[25] A.A. Gokhale, J.A. Dumesic, M. Mavrikakis, J. Am. Chem. Soc. 130 (2008) 1402-1414.

[26] A.D. Becke, J. Chem. Phys. 98 (1993) 5648-52.

[27] P. Perdew, Y. Wang, Phys. Rev. B 45 (1992) 13244-13249.

[28] T. Yumura, T. Nanba, H. Torigoe, Y. Kuroda, H. Kobayashi, Inorg. Chem. 50 (2011) 6533-6542.

[29] T. Yumura, A. Oda, H. Torigoe, A. Itadani, Y. Kuroda, T. Wakasugi, H. Kobayashi, J. Phys. Chem. C. 118 (2014) 23874-23887.

[30] T. Yumura, M. Kumondai, Y. Kuroda, T. Wakasugi, H. Kobayashi, RSC Adv. 7 (2017) 4950-4959.

[31] S. Zhao, X. Tian, J. Liu, Y. Ren, J. Wang, Comput. Theor. Chem. 1055 (2015) 1-7.

[32] X. Xia, X. Kuang, C. Lu, Y. Jin, X. Xing, G. Merino, A. Hermann, J. Phys. Chem. A 120 (2016) 7947-7954.

[33] M.J. Frisch, G.W. Trucks, H.B. Schlegel, G.E. Scuseria, M.A. Robb, J.R. Cheeseman, J.A. Montgomery Jr., T. Vreven, K.N. Kudin, J.C. Burant, J.M. Millam, S.S. Iyengar, J. Tomasi, V. Barone, B. Mennucci, M. Cossi, G. Scalmani, N. Rega, G.A. Petersson, H. Nakatsuji, M. Hada, M. Ehara, K. Toyota, R. Fukuda, J. Hasegawa, M. Ishida, T. Nakajima, Y. Honda, O. Kitao, H. Nakai, M. Klene, X. Li, J.E. Knox, H.P. Hratchian, J.B. Cross, V. Bakken, C. Adamo, J. Jaramillo, R. Gomperts, R.E. Stratmann, O. Yazyev, A.J. Austin, R. Cammi, C. Pomelli, J.W. Ochterski, P.Y. Ayala, K. Morokuma, G.A. Voth, P. Salvador, J.J. Dannenberg, V.G. Zakrzewski, S. Dapprich, A.D. Daniels, M.C. Strain, O. Farkas, D.K. Malick, A.D. Rabuck, K. Raghavachari, J.B. Foresman, J.V. Ortiz, Q. Cui, A.G. Baboul, S. Clifford, J. Cioslowski, B.B. Stefanov, G. Liu, A. Liashenko, P. Piskorz, I. Komaromi, R.L. Martin, D.J. Fox, T. Keith, M.A. Al-Laham, C.Y. Peng, A. Nanayakkara, M. Challacombe, P.M. W. Gill, B. Johnson, W. Chen, M.W. Wong, C. Gonzalez, J.A. Pople, Gaussian 03, Revision B.03, Gaussian Inc., Pittsburgh, PA, 2003.

[34] X. Zhang, D. Meng, X. Li, L. Meng, Z. Sun, J. Organomet. Chem. 769 (2014) 106-111.

[35] Y. Yang, S. Hu, Y. Fang, H. Wei, S. Hu, D. Wang, L. Yang, H. Zhang, S. Luo, Polyhedron 95 (2015) 86-90.

[36] A. Lupan, R.B. King, Inorg. Chim. Acta. 397 (2013) 83-87.

[37] V.T. Cong, L.K. Huynh, J.C. Jiang, N.T.A. Nhung, P.V. Tat, Comput. Theor. Chem. 1081 (2016) 62-70.

[38] N. Liu, L. Guo, Z. Cao, A. Li, X. An, Prot. Met. Phys. Chem. Surf. 52 (2016) 387-398.

[39] Z. Xiao-feng, X. Ji-long, M. Yue, Q. Meng-dan, X. Sheng-jie, N. Zhe-ming, J. Fuel. Chem. Technol. 45 (2017) 1473-1480.